Energy 266 (2023) 126410

Contents lists available at ScienceDirect

Energy

journal homepage: www.elsevier.com/locate/energy

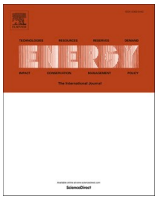

A new quasi-dynamic load flow calculation for district heating networks

Josef Steinegger *, Stefan Wallner, Matthias Greiml, Thomas Kienberger

Chair of Energy Network Technology, University of Leoben, Franz-Josef Straße 18, 8700, Leoben, Austria

ARTICLE INFO

Keywords:
Quasi-dynamic approach
Lagrangian specification approach
District heating network
Heat load flow calculation
Improved plug-flow method

ABSTRACT

District heating networks can serve as large heat reservoirs due to thermal inertia. To analyse the behaviour of these networks, a load flow calculation must be performed. There are three basic approaches available for this purpose. One is the steady-state approach, which cannot consider the temporal temperature distribution. Another one is the dynamic approach that considers the thermal inertia of district heating networks, but it has a high computation time. The presented method uses a quasi-dynamic approach, which can provide a faster calculation time than dynamic approaches and can also consider thermal inertia. This method is based on a Lagrangian specification approach which shows better performance than Eulerian specification approaches but is more complex to implement. The validation of the method indicates that the accuracy is high and, therefore, acceptable. The computation time of the method is several times faster than dynamic approaches and slightly slower than steady-state approaches. However, with quasi-dynamic approaches, it has not been possible to compute networks of arbitrary size and complexity. With the method described in this paper, this is now possible. Furthermore, due to its properties, the method can be well integrated into calculation methods of multi-energy-systems.

Nomenclature

A. Greek letters	
η	Kinematic viscosity
λ	Friction factor
ρ	Density
B. Parameters	
g	Reciprocal of the resistance value
R	Resistance value
Re	Reynolds number
$\dot{V}$	Volume flow
d	Pipe diameter
k	Wall roughness
l	Pipe length
Δp	Pressure drop
c_p	Heat capacity
$\dot{Q}$	Consumed or generated power
ΔT	Temperature difference
u	Thermal transmittance coefficient
C	Circumference
x	Moved distance
T	Temperature
Δt	Duration of a time step
A	Cross section of a pipe
n	Number of nodes
y'	Calculated value
y	Measured value
z	Current time step
N	Number of time steps
C. Abbreviation	
NEFI	New Energy for Industry
IPCC	Intergovernmental Panel on Climate Change
EU	European Union
DHN	District Heating Networks
LFC	Load Flow Calculation
MAPE	Mean Absolute Percentage Error
MSL	Modelica Standard Library
KPI	Key Performance Indicator
MES	Multi-Energy-Systems
CPU	Central Processing Unit
D. Indices	
k	Iteration step
g	Iteration step
i	Node
j	Node
FF	Feed flow
RF	Return flow
meas	Measured

* Corresponding author.
E-mail address: josef.steinegger@unileoben.ac.at (J. Steinegger).

https://doi.org/10.1016/j.energy.2022.126410
Received 24 May 2022; Received in revised form 4 November 2022; Accepted 10 December 2022
Available online 14 December 2022

1. Introduction

According to the Intergovernmental Panel on Climate Change (IPCC) report published in 2022, the impact of climate change on the structure of ecosystems is huge. The regions in Europe and North America are particularly affected [1]. As part of the European Green Deal, the European Union (EU) has set itself the goal of achieving climate neutrality by 2050 [2]. As a member of the EU, Austria has set itself even more ambitious goals, namely, to achieve climate neutrality by 2040. By separating Austria's energy consumption into the sectors of heat, electricity and mobility, the share of the heat sector was around 50% [3] in 2019. Due to the enormous importance of the heating sector, according to the actual government program, Austria plans to reduce CO_2 emissions, among others, by expanding district heating networks (DHN) in regions with a high density of heat consumers [4]. The preferred heat sources for sustainable heat networks are primarily renewable and industrial waste heat sources. An important reason is that industrial waste heat can replace additional oil and gas heating, thereby reducing CO_2 emissions [5,6]. Therefore, supraregional heat transfer lines may be required to connect industrial waste heat sites with consumers. These lines will show high losses. To compensate for them, heat pumps, thermal storage, or heating plants may be needed to raise the temperature of the water to acceptable values [7]. Due to the high heat capacity of water and the slow volume flow (0.2–4.0 m/s) [8] in DHN, these systems can also store heat for several hours. This property means that they can be used for load shifting in electric grids, e.g. with the help of heat pumps [9]. This will be particularly necessary for our future energy systems with a high proportion of renewable, fluctuating energy producers. Therefore, when planning district heating networks, not only the heating sector must be examined [10]. It is also necessary to consider the other sectors simultaneously to consider the complex interrelationships between the different energy carriers.

1.1. State-of-research

There are several approaches to calculate and simulate the load flow of district heating networks described in the recent literature. For different calculation purposes, considering the temporal temperature distribution within the spatially resolved network is of particular interest. In this regard, the load flow calculation (LFC) can be divided into various approaches. The temporal temperature distribution is not considered in steady-state approaches but is regarded in dynamic approaches [9]. This means that dynamic approaches include the temporal temperature distribution due to different temperature inputs in each pipe section and node over time. There is also a quasi-dynamic approach. The difference between quasi-dynamic and dynamic approaches is that in quasi-dynamic approaches, the transmission delay is only considered at each node [11]. The methods described in the literature can be categorised according to their basic approach, as shown in Table 1. In addition to the approaches listed in the table, there is also an intermediate category (quasi-steady-state) described by Dancker and Wolter [9,12]. The method described therein contains the essential points of a quasi-dynamic approach and is therefore considered as a quasi-dynamic approach in this paper.

In heat load flow calculations, thermal- and hydraulic calculations can be coupled or decoupled. The calculation equations are split between a hydraulic and a (dynamic) thermal part if the chosen method uses a decoupled approach. In a coupled approach, the equations for the hydraulic and the thermal parts are combined into one equation [9].

1.1.1. Steady-state approaches

Steady-state approaches can be coupled or decoupled. Both approaches generally use the Newton-Raphson method or another iterative procedure to calculate the heat load flow. In the decoupled calculation approach the hydraulic part of the load flow is calculated first. This is usually done with the Newton-Raphson method [9] or the Jacobi method [41]. The thermal part can be calculated with the calculated mass flow rates from the hydraulic calculation. Due to the decoupled approach, the matrix required to calculate the hydraulic part is smaller than for a coupled approach. This leads, on the one hand, to a faster calculation of the matrix but, on the other hand, to more iteration steps in the calculation. With the coupled approach, the heat load flow can be calculated in a single equation using the Jacobian matrix in combination with the Newton-Raphson method. This leads to fewer iteration steps but to a higher computation time of the matrix due to the larger matrix [9]. Steady-state approaches are usually applied to calculate multi-energy networks because they require little computational power [30].

Table 1
Classification of the different methods according to their approach.

Method	Approach		
	Steady-state	Quasi-dynamic	Dynamic
[13]	X		
[14]	X		
[15]	X		
[16]	X		
[17]	X		
[18]	X		
[19]	X		
[20]	X		
[21]	X		
[22]	X		
[23]	X		
[24]	X		
[9]		X	
[25]		X	
[26,27],[a]		X	
[28]		X	
[29,30]		X	
[31]		X	
This Paper		**X**	
[32,33]			X
[34]			X
[35]			X
[36]			X
[37]			X
[38]			X
[39]			X
[40]			X
[11]			X

[a] District cooling systems.

1.1.2. Quasi-dynamic approaches

A quasi-dynamic or a dynamic approach can be based on a Lagrangian or an Eulerian specification of the flow field. These two specifications describe the way of looking at a water segment motion. The difference between these two is that in the Eulerian specification, a specific location in the network is observed through which water segments flow as time passes. In contrast, in the Lagrangian specification, the observer moves through the network with water segments as time passes [9]. In quasi-dynamic approaches, the transmission delay is considered and stored only at the nodes of the considered network [11]. In the method presented by Benonysson [31], the quasi-dynamic approach is based on a "node method" that determines the temperature, considering the transmission delay at the nodes. This method is based on an Eulerian specification approach and reduces the numerical diffusion [9] and the computational effort [29] compared with some dynamic approaches. But the numerical diffusion increases with strong mass flow changes [9].

The so-called improved quasi-steady-state approach, introduced by Dancker and Wolter [9], uses an extended steady-state approach to calculate the heat load flow. For this purpose, they use a coupled calculation approach, combining the hydraulic and thermal parts in one equation in the Jacobian matrix. Therefore, they introduce a

temperature-gradient which is integrated into the equation for the hydraulic and thermal parts. This allows the steady-state approach to be upgraded to some extent to a quasi-dynamic approach. In addition, the coupled approach enables high accuracy and leads to fewer iteration steps, which increases computational efficiency, according to the authors. However, there is one limitation noted with this method. The Investigation of a highly meshed network with short pipes and large time step durations can cause temperatures at nodes that increase too fast and decrease too slowly. This is because the temperature-gradient method only considers a single change between two time steps. Therefore, the mixing temperature from a node more than one node back cannot be considered in a time step under consideration. This means that the proposed method offers only limited accuracy in such situations [9].

Another quasi-dynamic method uses a Lagrangian specification approach, as shown in Ref. [26], for district cooling networks. With this approach, water segments are tracked across the entire network. In some literature sources (e.g. Refs. [26–28]), this method is called the plug-flow method. For this purpose, a hydraulic model is created to obtain information about the mass flow and the pressure differences if a predefined system does not give this. The hydraulic model is usually based on a steady-state approach since the dynamic effects can be neglected due to the high propagation speed of pressure. The water segments for the thermal part of the calculation are moved through the pipes and split or merged at nodes with more than one outlet or inlet pipe. In this way, the temperature profile and flow path of the segments in each pipe of the network can be tracked so that the dynamic thermal behaviour of the network at each node can be determined as the segments pass through the node of interest. To prevent mixing two or more water streams in a single pipe from resulting in too many segments, only a maximum number of segments is allowed in one pipe. If the number of segments exceeds the maximum number, adjacent segments with the closest temperature are combined into one equivalent segment. This can prevent a too large calculation time due to too many segments. The accuracy is comparable to dynamic approaches with the advantage that the computation time is faster and the calculation does not involve artificial diffusion [26].

Leitner et al. [30], based on the results of [29], use a plug flow method to calculate DHN.

Dénarié et al. [28] present an improved plug-flow method which uses the “method of characteristics” to determine the dynamic behaviour at nodes.

However, [26,28–30] do not describe their approach for large, highly branched networks.

1.1.3. Dynamic approaches

Dynamic approaches typically use an Eulerian specification approach. There exist different methods for this specification like the “element method” [32,39], the above-described “node method” [31] and other methods or sub-methods like e.g. the “finite difference methods” [34,36,37], the “function method” and the “method of characteristics” [28]. [9] With the element method, the pipe length is decomposed into finite elements with a predefined length. These elements can be used to calculate the temperature as a function of the location in the pipe and the time step by using the parameters of the previous time step [32]. Depending on the number of elements, the calculation time scales linearly with it, and the accuracy is inversely proportional to the square of the element length [29]. The comparison of the computation times in Ref. [29] shows that dynamic approaches have a computation time several times higher than the other approaches.

1.1.4. Comparison of the approaches

The literature review shows that quasi-dynamic (except the described quasi-steady-state approach from Dancker et al. [9]) and dynamic approaches are always designed as decoupled calculations. A dynamic approach requiring only one equation, resulting in a coupled calculation, would be superior because it would allow the realistic calculation of considered DHN with a fast calculation time [9]. However, such a method currently does not exist. The properties of each different approach are shown in Table 2.

1.2. Research Need

As shown in Chapter 1.1, several approaches already exist to calculate the load flow in district heating systems. The presented method in this paper must meet several requirements:

- An easy implementation into existing multi-energy-system (MES) simulation frameworks, especially the HyFlow framework [42].
- A hydraulic calculation equivalent to an existing gas load flow calculation that uses a Jacobi method to calculate the nodal pressure to obtain solutions that are comparable in terms of accuracy.
- A calculation method which is fast enough to calculate multiple networks in an acceptable time frame.
- The possibility of taking temporal temperature distribution into account.
- Covering all types of network topologies, i.e., both small, highly branched networks and networks with long transmission lines.
- An accuracy that is largely independent of the step size.
- The consideration of typical elements of 3rd and 4th generation [43] heat networks, like classic suppliers and consumers, heat pumps, pressure pumps, throttles, thermal storage, and branch nodes in both the feed and return flow.
- A freely available code for integrating different operating strategies for the sequence of use of heat generators in district heating networks. Which could be added in future work

Due to the required versatility, which includes the creation of various operating strategies and the planned integration in HyFlow, conventional software cannot be used. According to Table 2, only the quasi-dynamic approach can meet all the requirements described. The calculation time of the dynamic approach is too high, and the steady-state approach does not consider the temporal temperature distribution. To avoid the described error in the method of Dancker and Wolter [9], only the remaining methods based on the quasi-dynamic approach are suitable for this work. As described in Chapter 1.1, the Eulerian specification approach proposed by Benonysson [31] can lead to numerical diffusion. The plug-flow methods presented in Refs. [26,28], which are based on the Lagrangian specification approach, are superior to the methods based on the Eulerian specification approach because these two methods have faster computation time, but the implementation is more complex [9]. Due to this factual situation, this work focuses on a Lagrangian specification approach similar to the existing plug-flow methods. Zhaoguang et al. [25] describe their Lagrangian specification approach only in minor detail. The method presented by Opplet et al. [26] is designed for radial district cooling networks and doesn’t consider meshed networks. However, Dénarié et al. [28] describe their method for heat transmission over long pipes very accurately, but with the

Table 2
Definition of the different approaches.

Feature	Approach		
	Steady-state	Quasi-dynamic	Dynamic
Consideration of thermal losses	Yes	Yes	Yes
Consideration of temporal temperature distribution	No	At nodes	Whole network
Fast calculation	Yes	Yes	No
High accuracy	Yes	Yes	Yes
Numerical diffusion	No	Yes/No[a]	Yes/No[a]
Calculation approach	Coupled/ Decoupled[a]	Coupled/ Decoupled[a]	Decoupled

[a] Depending on the method.

caveat that the work presented was not applied for an entire network and the problems that arise from it. Based on this state-of-the-art, the main contributions of this present paper are as follows:

- Introducing a quasi-dynamic approach using a Lagrangian specification approach to calculate entire district heating networks with any given structure.
- Incorporation of various district heating network elements, such as classic suppliers and consumers, heat pumps, pressure pumps, throttles, thermal storages, and branch nodes into the calculation.
- Solving the complex programming challenges of a LFC based on a Lagrangian specification approach when a water segment has to traverse a highly branched network within a time step.

2. Theoretical background

This research focuses on a quasi-dynamic load flow calculation based on a steady-state calculation. The fundamentals of the steady-state hydraulic approach are described in the work of Rüdiger et al. [41]. Here, a node potential algorithm for gas networks is used based on the node potential calculation method of electrical systems. This steady-state method enables the calculation of the mass flow $\dot{V}$ and the pressure drop Δp in the branches of gas networks. Therefore, a square, inverse conductance matrix $\overline{G}^{-1}$ is created with n rows and n columns, where n is the number of nodes in the network plus an additional row and column for the slack node (see Chapter 4 Fig. 5). The content of this matrix consists of the conductance g of each branch. Each conductance can be calculated as shown in Eqs. (2-1), where g is the reciprocal of the resistance value R.

$$g = \frac{1}{R} \tag{2-1}$$

The resistance value R can be calculated with the friction factor λ, which depends on the Reynolds number Re. As a first step, the Reynolds number can be calculated with Eqs. (2-2).

$$Re = \frac{4 \bullet \dot{V}}{\pi \bullet d \bullet \eta} \tag{2-2}$$

For laminar volume flows ($Re < 2320$), the friction factor can be calculated as shown in Eqs. (2-3).

$$\lambda = \frac{64}{Re} \tag{2-3}$$

With the Colebrook–White equation, the friction factor can be calculated for turbulent flows, as shown in Eqs. (2-4). A Newton-Raphson method can be used to solve this equation.

$$\frac{1}{\sqrt{\lambda}} = -2 \bullet log_{10}\left(\frac{2.51}{Re \bullet \sqrt{\lambda}} + \frac{k}{3.7 \bullet d}\right) \tag{2-4}$$

Finally, the resistance value can be determined with the calculated variables, the density ρ and the geometry pipeline factors l and d:

$$R = \frac{1}{g} = \frac{8 \bullet \rho \bullet \lambda}{\pi^2} \bullet \frac{l}{d^5} \tag{2-5}$$

Using the Darcy–Weisbach equation, as shown in Eqs. (2-6), the pressure drop in a pipeline between two nodes (Δp_{ij}) can be calculated. $\dot{V}_{ij}$ corresponds to the volume flow between those two nodes.

$$\Delta p_{ij} = \frac{1}{g_{ij}} \bullet \dot{V}_{ij}^2 = \frac{8 \bullet \rho \bullet \lambda_{ij}}{\pi^2} \bullet \frac{l_{ij}}{d_{ij}^5} \bullet \dot{V}_{ij}^2 \tag{2-6}$$

To compensate for the non-linearity of the Darcy–Weisbach Eqs. (2-6), the quadratic dependence on the volume flow must be converted into a linear dependence. For this purpose, the volume flow can be divided into a volume flow of the previous iteration step *k-1* and the current iteration step *k*. Thus, to calculate the pressure drop (shown in Eqs. (2-7)) for iteration step *k*, the volume flow from the previous iteration step *k-1* is required. Since there are no volume flows from the last iteration step in the first iteration step, the initial volume flows are used in this case. Using the Darcy–Weisbach equation (Eqs. (2-7)), the pressure drop in the pipe can be calculated in a few iteration steps.

$$\Delta p_{ij,(k)} = \frac{1}{g_{ij,(k-1)}} \bullet \dot{V}_{ij,(k)} = \frac{8 \bullet \rho \bullet \lambda_{ij,(k-1)}}{\pi^2} \bullet \frac{l_{ij}}{d_{ij}^5} \bullet \dot{V}_{ij,(k-1)} \bullet \dot{V}_{ij,(k)} \tag{2-7}$$

To illustrate the calculation of the node pressure $\Delta p_{i0,(k)}$ of each node, the following section explains the basics of the nodal potential method in a hydraulic network in more detail using an example network. This network is shown in Fig. 1 and has one supplier-, one slack-, and two consumer nodes. The incoming- or outgoing volume flow $\dot{V}_{i,(k)}$ at each node is described by its index with the node number *i*.

Fig. 2 shows the equivalent circuit of the sample hydraulic network. The horizontal conductance values $g_{ij,(k-1)}$ correspond to the reciprocal resistances $R_{ij,(k-1)}$ in the pipes between two nodes.

The vertical conductance values $g_{i0,(k)}$ multiplied with the pressure difference $\Delta p_{i0,(k)}$ of each node with respect to the environment (node 0) correspond to the incoming- or outgoing volume flows $\dot{V}_{i,(k)}$ at each node in the sample network as shown in Eqs. (2–8).

$$\dot{V}_{i,(k)} = g_{i0,(k)} \bullet \Delta p_{i0,(k)} \tag{2-8}$$

The equivalent circuit is used to set up the node equations, as shown in Eqs. (2-9).

$$\begin{aligned}
&Node1: \\
&g_{12,(k-1)} \bullet \left(\Delta p_{10,(k)} - \Delta p_{20,(k)}\right) - \dot{V}_{1,(k)} &&= 0 \\
&Node2: \\
&g_{12,(k-1)} \bullet \left(\Delta p_{20,(k)} - \Delta p_{10,(k)}\right) + g_{23,(k-1)} \bullet \left(\Delta p_{20,(k)} - \Delta p_{30,(k)}\right) + \dot{V}_{2,(k)} &&= 0 \\
&Node3: \\
&g_{23,(k-1)} \bullet \left(\Delta p_{30,(k)} - \Delta p_{20,(k)}\right) + \dot{V}_{3,(k)} &&= 0
\end{aligned} \tag{2-9}$$

These equations are transformed so that the node pressures are sorted, and the incoming- or outgoing volume flows $\dot{V}_{i,(k)}$ are on the right side of the equation, as shown in Eq. (2-10).

$$\begin{aligned}
&Node1: \\
&g_{12,(k-1)} \bullet \Delta p_{10,(k)} - g_{12,(k-1)} \bullet \Delta p_{20,(k)} &&= \dot{V}_{1,(k)} \\
&Node2: \\
&-g_{12,(k-1)} \bullet \Delta p_{10,(k)} + \left(g_{12,(k-1)} + g_{23,(k-1)}\right) \bullet \Delta p_{20,(k)} - g_{23,(k-1)} \bullet \Delta p_{30,(k)} &&= -\dot{V}_{2,(k)} \\
&Node3: \\
&-g_{23,(k-1)} \bullet \Delta p_{20,(k)} + g_{23,(k-1)} \bullet \Delta p_{30,(k)} &&= -\dot{V}_{3,(k)}
\end{aligned} \tag{2-10}$$

The system of equations in Eq. (2-10) is put into matrix form as shown in Eq. (2-11), which can be described by Eq. (2-12).

$$\begin{pmatrix} g_{12,(k-1)} & -g_{12,(k-1)} & 0 \\ -g_{12,(k-1)} & g_{12,(k-1)} + g_{23,(k-1)} & -g_{23,(k-1)} \\ 0 & -g_{23,(k-1)} & g_{23,(k-1)} \end{pmatrix} \bullet \begin{pmatrix} \Delta p_{10,(k)} \\ \Delta p_{20,(k)} \\ \Delta p_{30,(k)} \end{pmatrix} = \begin{pmatrix} \dot{V}_{1,(k)} \\ -\dot{V}_{2,(k)} \\ -\dot{V}_{3,(k)} \end{pmatrix} \tag{2-11}$$

$$\overline{G}_{(k-1)} \bullet \overline{X}_{node,(k)} = \overline{Z}_{node,(k)} \tag{2-12}$$

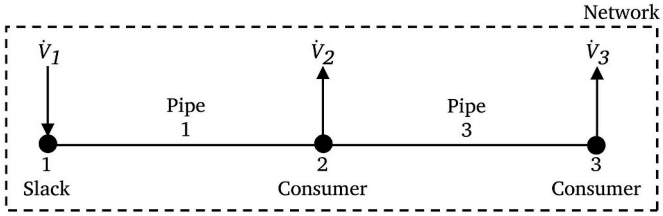

Fig. 1. Sample hydraulic network.

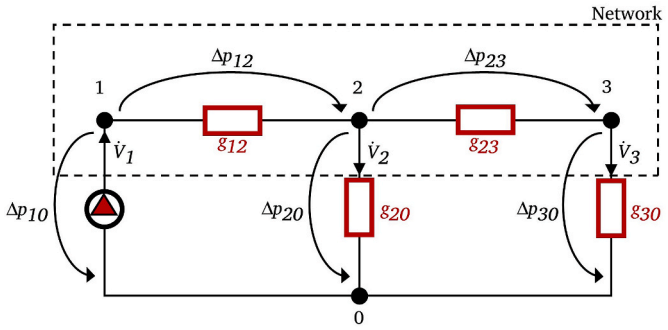

Fig. 2. Equivalent circuit of the sample hydraulic network.

With the incoming- or outgoing volume flows $\dot{V}_{i,(k)}$ of each node in the volume flow vector $\overline{Z}_{node,(k)}$, multiplied with the inverse conductance matrix $\overline{G}^{-1}_{(k-1)}$, the pressure $\Delta p_{i0,(k)}$ at each node can be calculated and stored in the pressure vector $\overline{X}_{node,(k)}$ as shown in Eq. (2-13). To consider the slack node in the calculation, the conductance matrix $\overline{G}_{(k-1)}$ and the vector $\overline{Z}_{node,(k)}$ need to be modified, as shown in Figs. 5 and 6 in Chapter 4.

$$\overline{X}_{node,(k)} = \overline{G}^{-1}_{(k-1)} \bullet \overline{Z}_{node,(k)} \tag{2-13}$$

The pressure drop $\Delta p_{ij,(k)}$ between two nodes can be calculated with the results from Eq. (2-13) as shown in the Eq. (2-14).

$$\Delta p_{ij,(k)} = \Delta p_{i0,(k)} - \Delta p_{j0,(k)} \tag{2-14}$$

The new volume flow $\dot{V}_{ij,(k)}$ for each pipe can be determined for each iteration step with the help of $\Delta p_{ij,(k)}$ as shown in (2-15).

$$\dot{V}_{ij,(k)} = sign\left(\Delta p_{ij,(k)}\right) \bullet \sqrt{\frac{\pi^2}{8 \bullet \rho \bullet \lambda_{ij,(k-1)}} \bullet \frac{d_{ij}^5}{l_{ij}} \bullet \left|\Delta p_{ij,(k)}\right|} \tag{2-15}$$

Using the equations described, the volume flow and the pressure can be calculated for each time step. Whereby the iteration must be carried out for each time step.

3. Overview methodology

The improved plug-flow method presented in this paper corresponds to a quasi-dynamic approach. This approach is divided into a hydraulic part for the feed- and return flow, a thermal part and a Lagrangian specification part, as shown in Fig. 3.

First, the hydraulic part for the feed- and return flow is calculated based on the approach of Rüdiger [41]. Second, in the thermal part, based on the results of the hydraulic part, the temperatures are calculated for the entire network in steady-state. Third, the water segments resulting from the steady-state calculation are shifted through the network using a Lagrangian specification approach to calculate the network's dynamic behaviour at each node. Finally, an overall iteration is performed over the steady-state and quasi-dynamic parts of the calculation until the calculated temperatures at each node of iteration step *g* converge to the temperatures of the previous iteration step *g-1*.

The LFC has been implemented in MATLAB® using a class programming approach. The following assumptions were made:

- The temperature and velocity profiles are axially symmetric inside a pipe section.
- There is no thermal stratification in the radial direction.
- There is no thermal diffusion in the axial direction.
- Water is considered as an incompressible and homogeneous fluid.
- The properties of the materials are constant.

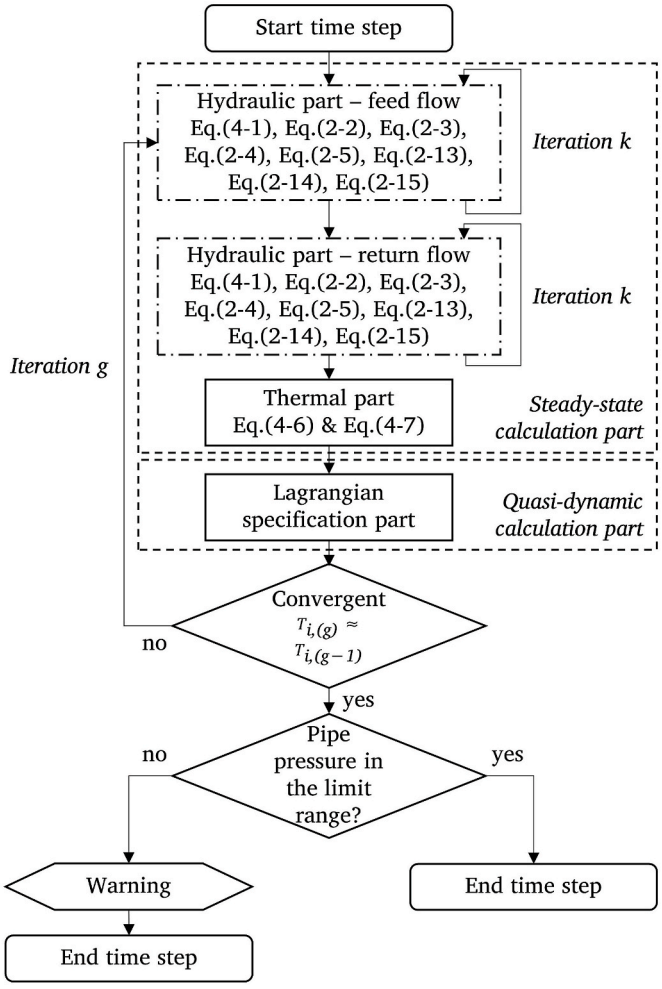

Fig. 3. Calculation method of the quasi-dynamic approach.

- The density, heat capacity, and kinematic viscosity of water were assumed to be temperature-independent quantities.

In addition, the thermal inertia of the pipe wall was neglected. This decision was made based on the results of Wang et al. [44]. It states that thermal inertia produces an error similar to the neglect of the temperature dependence of the specific heat capacity and is therefore negligible, especially for larger pipe diameters.

4. Steady-state calculation part

The steady-state calculation part is divided into the hydraulic part for the feed- and return flow and the thermal part. Each part corresponds to a decoupled calculation, with each part building on the previous one.

4.1. Hydraulic part – feed flow

As shown in Fig. 3, each hydraulic part has its iteration loop to calculate the pressure drop and volume flow of each pipe in the network. Fig. 4 shows this iteration loop in detail.

At the beginning of the hydraulic part, the input vectors $\overline{Z}_{node,(g-1)}$ and $\overline{X}_{node,(k)}$ and the conductance matrix $\overline{G}_{(k-1)}$ must be prepared for Eq. (2-13). The volume flow vector $\overline{Z}_{node,(g-1)}$ needs to be prepared only once for all iteration steps of *k* within one iteration step of *g*. Because of this, the described vector is defined by the iteration step *g* in the index. The other two variables need to be updated each iteration step of *k*. For this reason, these variables are defined by the iteration step *k* in the index.

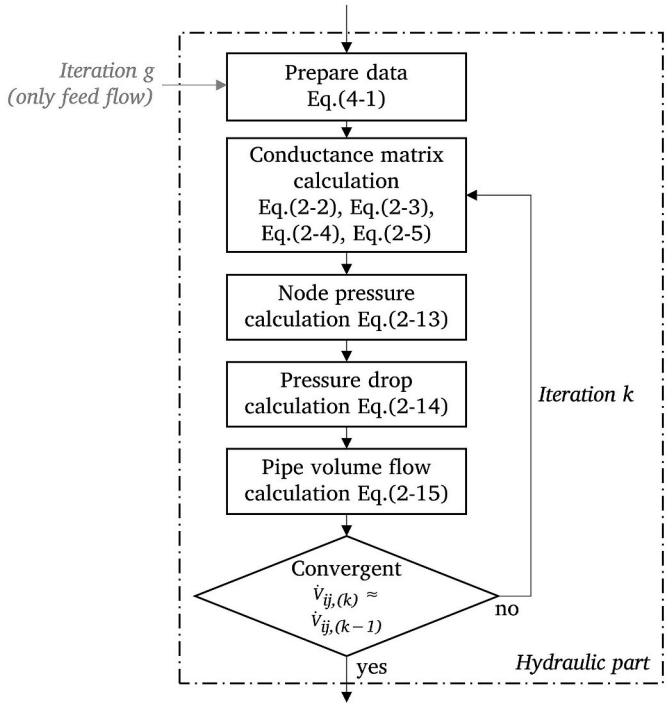

Fig. 4. Development of the heat LFC from the hydraulic LFC.

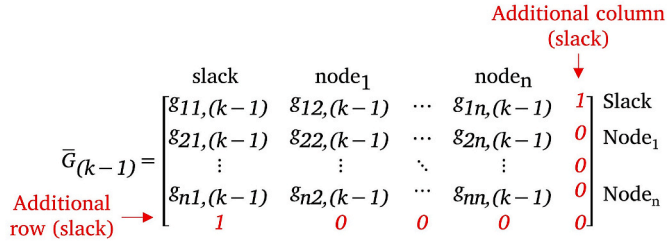

Fig. 5. Conductance matrix (slack).

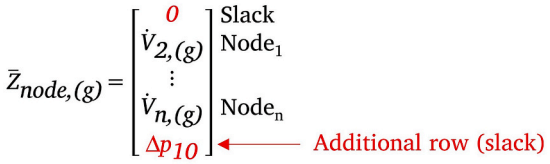

Fig. 6. Vector Z (slack).

The vector $\bar{Z}_{node,(g-1)}$ is filled with the volume flows $\dot{V}_{i,(g-1)}$ of the individual nodes *i*. $\dot{V}_{i,(g-1)}$ can be calculated from the consumer- or generation power $\dot{Q}_i$ for each node of the considered network for the considered time step. Depending on whether the node is a consumer or a supplier, the temperature change $\Delta T_{i,(g-1)}$ in Eqs. (4-1) is calculated differently. If the node is a consumer, the upper temperature is taken from the calculated feed flow from the previous iteration step *g-1,* and the lower temperature corresponds to the predefined return flow temperature of the consumer. In the case of suppliers, the predefined supplier feed flow temperature is used as the upper temperature, and the calculated temperature of the return flow from the previous iteration step *g-1* is used as the lower temperature. In the first iteration step, *g*, the return flow temperature is estimated for the supplier, and the feed flow temperature is estimated for the consumer. Finally, the node volume flow can be calculated with Eqs. (4-1).

$$\dot{V}_{i,(g-1)} = \frac{\dot{Q}_i}{\rho \bullet c_p \bullet \Delta T_{i,(g-1)}} \tag{4-1}$$

Furthermore, each hydraulic load flow calculation needs a slack node that defines the basic system pressure. This basic system pressure can be defined by a heat supplier in the feed flow. To calculate the total load flow of the considered network, either the pressure or the volume flow for each node can be used as input parameters in Eq. (2-13) for the volume flow vector $\bar{Z}_{node,(g-1)}$. If the pressure is given (as it is for slack nodes), the volume flow gets calculated for the considered node in the node pressure vector $\bar{X}_{node,(k)}$. To consider this, the slack node (and each node with a given pressure) requires an additional entry in the volume flow vector $\bar{Z}_{node,(g-1)}$ and the conductance matrix $\bar{G}_{(k-1)}$. Therefore, an extra row and column with zeros must be added to the conductance matrix $\bar{G}_{(k-1)}$. Afterwards, the value "*1*" must be set in the place of the slack, as shown in Fig. 5.

Also, the given pressure (for the slack node or any other node with a given pressure) has to be added as an additional row to the volume flow vector $\bar{Z}_{node,(g-1)}$. In addition, the volume flow at the slack has to be defined as zero, as shown in Fig. 6. In this way, the volume flow of the slack-node (or any other node with a given pressure) can be calculated in the node pressure vector $\bar{X}_{node,(k)}$.

Once the described variables are defined, the hydraulic part can be calculated using the equations listed in Fig. 4.

4.2. Hydraulic part – return flow

The hydraulic part of the feed flow and the return flow has to be linked because the return flow calculation needs the input data of the feed flow. In the return flow, the node with the lowest pressure in the feed flow part, minus the pressure losses of the corresponding heat exchanger, is the slack node. Depending on the consumer behaviour of each time step, this slack node of the return flow may change.

After the slack node is defined, the hydraulic calculation for the return flow can be calculated the same way as the hydraulic part of the feed flow, including the district heating elements. The initialisation data is the same as the data of the feed flow, except that a supplier in the feed flow is a consumer in the return flow, and a consumer in the feed flow is a supplier in the return flow. As a result, the signs in the volume flow vector $\bar{Z}_{node,(k)}$ change according to Eqs. (4-1). This is because the input parameter $\dot{Q}_i$ (consumer- or generation power) changes its sign due to the described change of supplier and consumer.

4.2.1. Integration of district heating network elements

The integration of the different elements directly affects the hydraulic and thermal part of the calculation, as they affect the pressure and the temperature. Due to these changes, the quasi-dynamic calculation part is only indirectly influenced. Since the Lagrangian specification part uses only the data of the steady-state part, as described in Chapter 5. There are three different system topologies to implement suppliers in a district heating network [44]. One possibility is to take the water from the return flow and feed it into the feed flow after heating it (Fig. 7a), which is also the most common approach. Another way is to take the water from the return flow and feed it back into the return flow (Fig. 7b). The last option is to take the water from the feed flow and feed it back into the feed flow (Fig. 7c).

To integrate the different hydraulic circuits in the hydraulic part of the calculation, the input parameters of Eq. (2-13) must be adapted. There are two possible ways to implement the hydraulic circuit presented in Fig. 7a, depending on whether it is a slack node or a common node. As already mentioned, the slack node is responsible for the basic pressure in the network, and it is integrated into the calculation as described in Figs. 5 and 6. Assuming that the pressure of the node is not given, the volume flow can be calculated from Eqs. (4-1). In that case, it

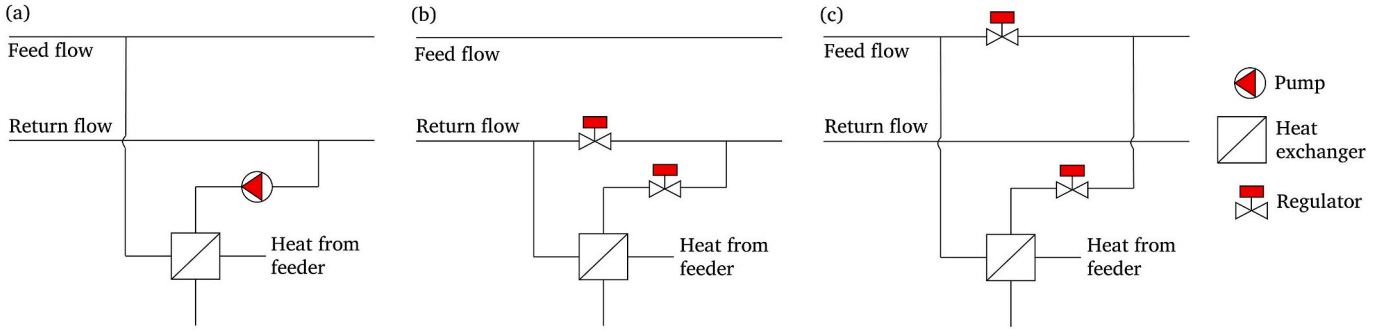

Fig. 7. Hydraulic circuits for heat feeders: (a) return flow – feed flow; (b) return flow – return flow; (c) feed flow – feed flow [44].

depends on the used signs of the volume flow in the volume flow vector $\overline{Z}_{node,(g-1)}$ whether it is an inflow (supplier) to the network or an outflow (consumer) from the network.

In the load flow calculation the hydraulic circuit from Fig. 7b and c is realised identically. The difference between these two is that the first is implemented in the hydraulic part of the return flow, and the second is implemented in the feed flow. These types are typical for power-to-heat applications like heat pumps, but conventional heat suppliers can also be used this way. In the LFC, such nodes are divided into two nodes. For this purpose, the node is split into an outflow (consumer) and an inflow (supplier) node, as shown in Fig. 8.

The pressure loss Δp_{23} between nodes 2 and 3 in Fig. 8 equals the predefined pressure drop in the heat exchanger. In this case, the following conditions are fulfilled:

$$|\dot{V}_2| = |\dot{V}_3| \tag{4-2}$$

$$\dot{V}_{12} = \dot{V}_{34} \tag{4-3}$$

$$\dot{V}_{12} = \dot{V}_2 + \dot{V}_{23} \tag{4-4}$$

$$\Delta p_{30} = \Delta p_{20} - \Delta p_{23} \tag{4-5}$$

To consider these equations, the outflow node is treated like a consumer and the inflow node as a standard supplier node for the observed hydraulic part in the load flow calculation. If the hydraulic circuit node is made according to Fig. 7b, the hydraulic part for the feed flow has no node at this point and vice versa for the hydraulic part for the return flow according to Fig. 7c. To consider the pressure drop between these two nodes, one row and one column with zeros, similar to the slack node, need to be added to the conductance matrix $\overline{G}_{(k-1)}$. The value "*-1*" must be inserted in the place of the outflow node, and the value "*1*" in the area of the inflow node, as shown in Fig. 9.

In addition to this, the pressure drop value $\Delta p_{12,(k)}$ must be added to the volume flow vector $\overline{Z}_{node,(k)}$ (Fig. 10).

The integration of pumps and throttles follows the same rules as the described hydraulic circuit according to Fig. 8, but there is no volume flow at the supplier (inflow)- or consumer (outflow) node. For this purpose, the volume flow from the in- and outflow node in the vector

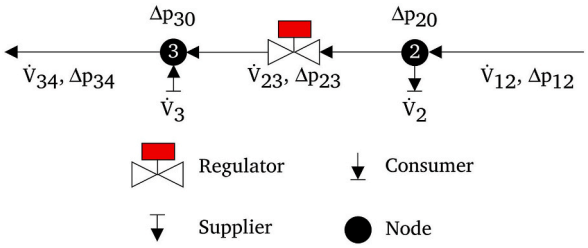

Fig. 8. Realization of feeder circuits according to Fig. 7b and c in the load flow calculation.

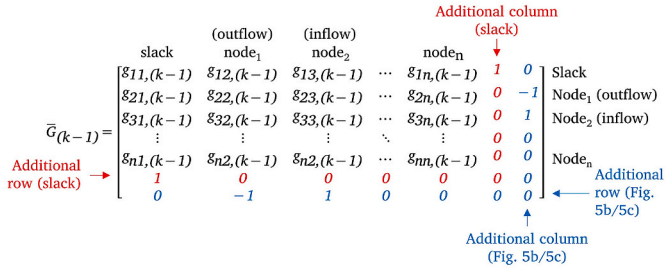

Fig. 9. Conductance matrix (slack + Fig. 7b/c).

$$\overline{Z}_{node,(g-1)} = \begin{bmatrix} 0 \\ -\dot{V}_{1,(g-1)} \\ \dot{V}_{2,(g-1)} \\ \vdots \\ \dot{V}_{n,(g-1)} \\ \Delta p_{10} \\ \Delta p_{12} \end{bmatrix} \begin{matrix} \text{Slack} \\ \text{Node}_1\ \text{(outflow)} \\ \text{Node}_2\ \text{(inflow)} \\ \\ \text{Node}_n \\ \leftarrow \text{Additional row (slack)} \\ \leftarrow \text{Additional row (Fig. 5b/5c)} \end{matrix}$$

Fig. 10. Vector Z (slack + Fig. 7b/c).

$\overline{Z}_{node,(g-1)}$ in Fig. 10 is set to zero. The conductance matrix $\overline{G}_{(k-1)}$ is built the same way as shown in Fig. 9.

For thermal storage integration, the storage operation strategy must be defined before the load flow calculation starts. Depending on this, the heat store can be treated as an ordinary consumer or a supplier, which is set up according to Fig. 7a.

To implement branch nodes, the volume flow of these nodes in the volume flow vector $\overline{Z}_{node,(g-1)}$ must be zero.

The described elements influence the thermal part of the calculation due to the temperature increase caused, for example, by suppliers (see Fig. 8).

4.3. Thermal part

The thermal part can be calculated with the input parameters of the hydraulic part. For this purpose, some additional equations are required. The following part deals with the technical details of the calculation of the temperatures in the entire network. Eq.s (4-6) based on [45] is applied to calculate the temperature of each node in the feed- and return flow. Where u is the thermal transmittance coefficient, x is the distance travelled, and C is the circumference of the pipe.

$$T_{node\ i+1} = (T_{node\ i} - T_{ambient}) \bullet e^{\frac{-u \bullet C \bullet x}{c_p \bullet \rho \bullet \dot{V}}} + T_{ambient} \tag{4-6}$$

A recursive method is used for this purpose, which is explained in Fig. 11. In the shown example a network with four nodes is given. The

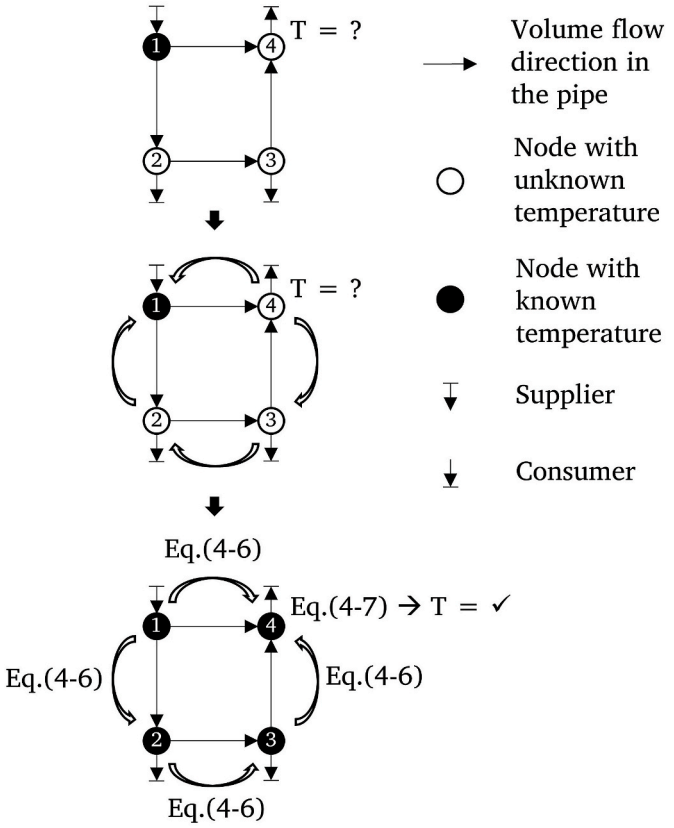

Fig. 11. Recursive method.

arrows indicate the direction of the volume flow. In the case described, the temperature of node 4 shall be determined (step 1 in the figure). For this purpose, the method follows the volume flow back (starting at node 4) until a node with a given temperature is found (step 2 in Fig. 11). When a node with a given temperature is found (in the described case, node 1), the algorithm calculates the temperatures of all nodes on the path back to node 4 by using Eq.s (4–6), as shown in step 3 in the figure. Regarding this, the temperature at node 4 can be calculated now.

For nodes with more than one inflow (node 4 in Fig. 11), the node temperature T_{node} can be calculated using a volume flow weighted temperature calculation as shown in (4-7).

$$T_{node} = \frac{T_{inflow,1} \bullet \dot{V}_{inflow,1} + \ldots + T_{inflow,n} \bullet \dot{V}_{inflow,n}}{\dot{V}_{inflow,1} + \ldots + \dot{V}_{inflow,n}} \tag{4-7}$$

Once the temperatures of all nodes are determined, the steady-state calculation part is completed.

5. Quasi-dynamic calculation part

To extend the presented steady-state approach (Chapters 2 and 4) to a quasi-dynamic approach, a plug-flow method based on a Lagrangian specification approach is implemented in the following part. The next chapter describes this part covering all the difficulties that can occur when considering an entire network.

5.1. Lagrangian specification part

An example of applying the Lagrangian specification approach is to track chemicals in water distribution systems based on water segments [46]. These water segments, described by Munavalli et al. [46], can be adapted to the heat load flow calculation. This chapter is divided into the sections "Description of a temperature batch", "Transport of batches in pipelines", "Behaviour of batches at nodes", and "A recursive algorithm to calculate highly meshed networks". Each section explains a different feature of the developed plug-flow method.

5.1.1. Description of a temperature batch

The main characteristic of a water segment in a heat network is the temperature. This is why these segments will subsequently be referred to as "temperature batches" in this paper. A temperature batch has different characteristics, as shown in Fig. 12.

Temperature batch: It is an imaginary finite-volume of water (batch) inside a pipe. These batches are limited at both ends by a separator, which has different characteristics. A temperature batch moves with a speed that depends on the flow velocity in the considered pipe and the considered time step. Batches are independent of each other.

Separator: There is a separator at the rear (rear separator) and at the front (front separator) end of a batch, the description of rear and front depends on the flow direction, as shown in Fig. 12. It is a line that contains information about the actual pipe, the temperature and the exact position where the considered line is at the considered time. It also separates one batch from another.

5.1.2. Transport of batches in pipelines

This section describes the calculation of batch movements in pipelines. Fig. 13 shows the time history of a pipe over several time steps:

Time step 1: The batches (b_1 in Fig. 13) for the entire network must be added in the first time increment. At this stage, these batches correspond to the results of the steady-state part. This also means that there is only one batch in each pipe of the network at this time.

Time step 2: The batch from time step 1 (b_1) moves forward by the distance Δx_{01} (Eq.s (5-1)), and the resulting gap must be filled by a new batch (b_2). The length of the new batch is determined by the volume flow rate of the pipe in time step 2, as shown in Eq.s (5-2), where A is the cross-section of the pipe and Δt is the duration of the time step.

$$\Delta x_{01} = x_1 - x_0 \tag{5-1}$$

$$\Delta x_{01} = \frac{\dot{V}_2 \bullet \Delta t}{A} \tag{5-2}$$

To calculate the front temperature T_{F2} of batch b_2, Eqs. (4-6) is needed. The front temperature is always the temperature of the batch at the front separator. The general Eqs. (4-6) shows that T_{F2} depends on the volume flow $\dot{V}_2$ and the distance travelled Δx_{01}.

Time step 3: A new batch is added similarly to time step 2. In the following time steps, only batch b_2 is described as an example for all other batches. The front temperature of this batch is calculated the same way as in time step 2. The distance travelled depends on the volume flow $\dot{V}_3$. At this time step also the rear temperature must be calculated. The rear temperature is always the temperature that prevails at the rear separator of the batch. This can be calculated analogous to the front temperature with Eqs. (4-6).

Time step 4 & 5: The rear temperatures are calculated as described in the other time steps. When batch 2 reaches the end of the pipe, the front temperature of batch 2 is calculated as in the previous time steps for time step 4. The calculation of the front temperature of batch 2 in the time step 5 is a particular case because it depends on the volume flow of the

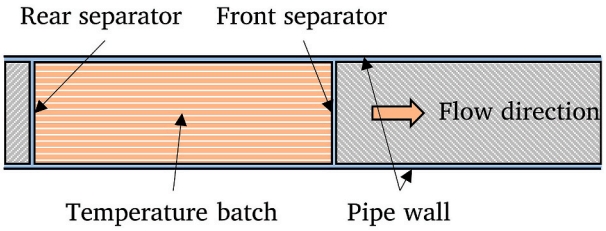

Fig. 12. Temperature batch.

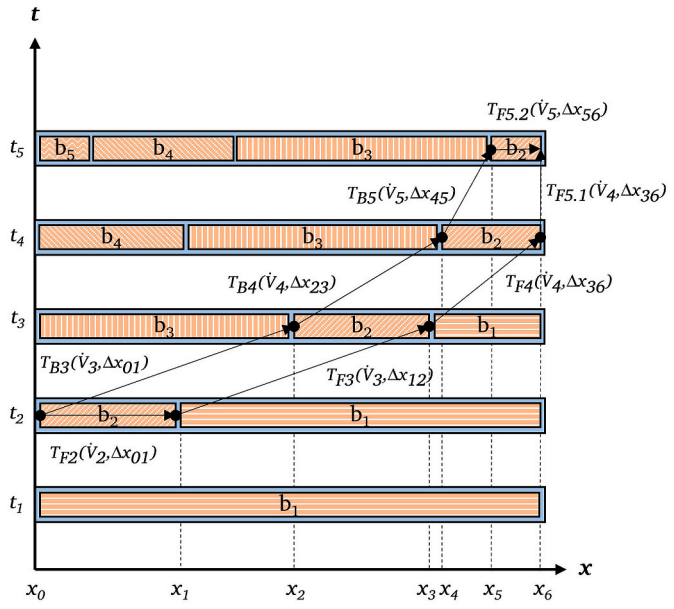

Fig. 13. Temperature batches.

time step 4 and 5. That is why the temperature is calculated from the average of both time steps, as shown in Eqs. (5-3).

$$T_{F5} = \frac{T_{F5.1} + T_{F5.2}}{2} \tag{5-3}$$

5.1.3. Behaviour of batches at nodes

Depending on the node, there are different effects on batches in a pipe. A temperature batch can be partitioned (Fig. 14 (a)), split (Fig. 14 (b)) or merged (Fig. 14 (c)) at nodes. The temperature of each batch in a pipe is always calculated, as described in Fig. 13.

Partitioning: A batch has to be partitioned if it reaches a node in the duration of a time step but does not leave the node in time. The new length of the new batch b_3 depends on the volume flow in pipe 2, as shown in Fig. 14 (a). The calculation of partitioning is described in more detail by Oppelt et al. [26].

Splitting: If a batch reaches a node with more than one outlet pipe, the batch must be split. As shown in Fig. 14 (b), the lengths of the newly created batches (b_2 and b_3) are individual and depend on the volume flow of the new pipes (pipes 2 and 3) into which they flow.

Merging: When two or more pipes end in one or more pipes, the batches must be merged. The batches of each pipe are merged at each outflow pipe to a new one. For this purpose, Eqs. (4-7) calculates the new volume flow weighted temperature. The new batches can only be as long as the shortest common length of the batches from the different pipes. Therefore, batches b_1 and b_2 are combined into a minimum of three batches in Fig. 14 (c) (depending on the other batches of pipes 1 and 2, which are not shown in the example for simplicity). All batches arriving at a node must be known to merge the batches into new ones.

To calculate the average temperature of a node, the temperature of each batch entering the node in the considered time step must be taken into account. Therefore, the average temperature is calculated time-weighted with the different temperatures of the arriving batches, as shown in (5-4). Where Δt_{bi} is the period in which the considered batch

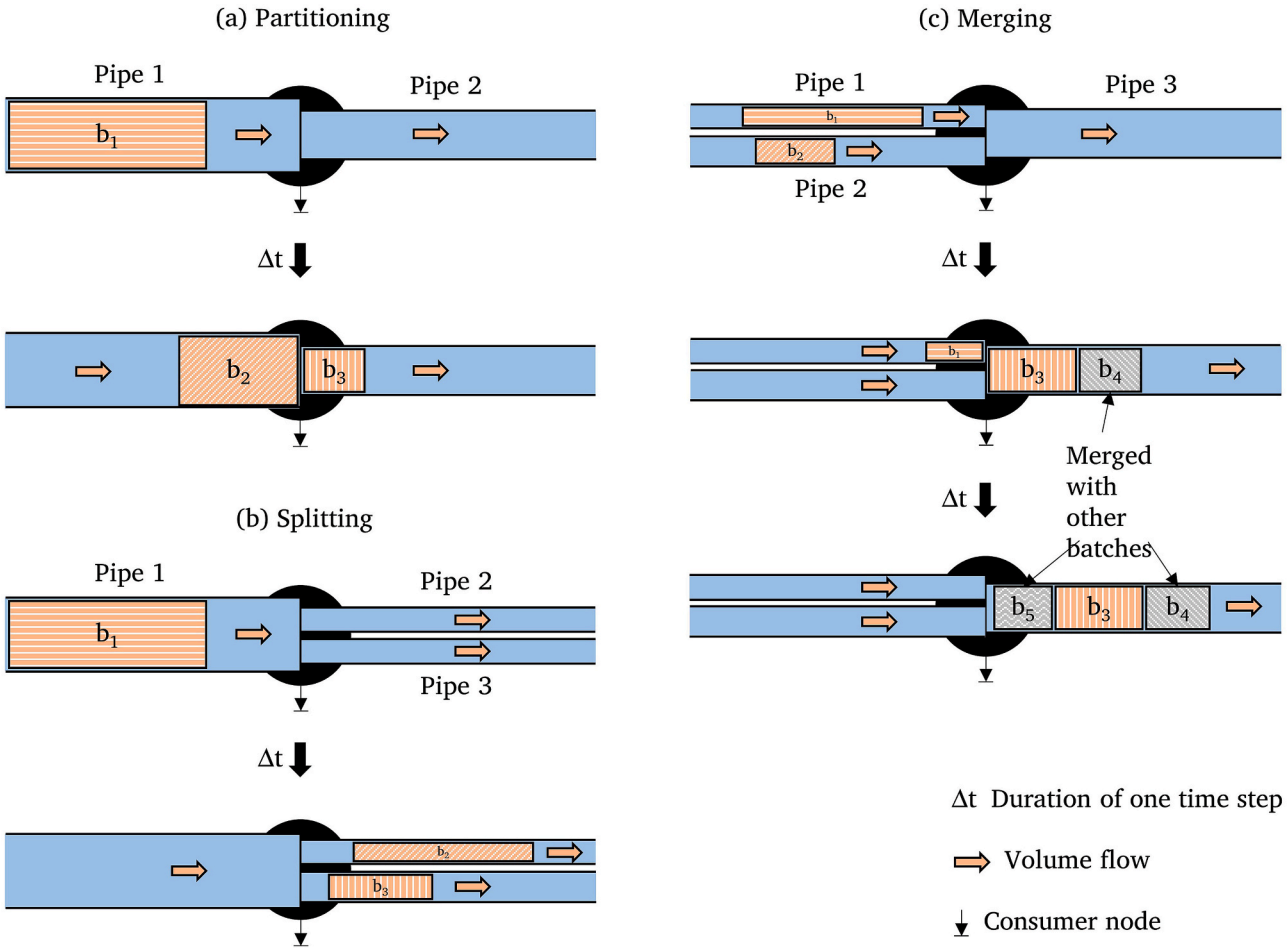

Fig. 14. Behaviour of temperature batches at nodes.

enters node *i*.

$$T_{inflow} = \frac{T_{b1} \bullet \Delta t_{b1} + \ldots + T_{bn} \bullet \Delta t_{bn}}{\Delta t} \quad (5\text{-}4)$$

5.1.4. A recursive algorithm to calculate highly meshed networks

The calculation for moving a batch in a network always starts with a random batch in the considered network. What happens after moving this batch to the next node depends on the structure of the node and the elapsed time. The batch can be partitioned, split or merged, as described in Section 5.1.3. In the case of merging, all the batches arriving at the node under consideration in the time step in question must be known. This issue leads to a complex task in a highly meshed network where a batch may pass through multiple nodes with more than one inlet or outlet pipe in the duration of a time step before it arrives at the node of interest. Therefore, a recursive algorithm must be added to the load flow calculation. The goal of this recursive method is to find all possible batches arriving at the considered node during the duration of a time step. This algorithm can be divided into three main parts, the investigation-, the pre-calculation- and the actual calculation part, as shown in Fig. 15.

Investigation part: In this part, the algorithm calculates the maximum distance (in the same way as Eqs. (5-2) does) that a batch can be away from the node to reach the node in one time step. If the algorithm finds another node with a merging character within this distance, that has not been calculated up to this point, the recursive algorithm must first be applied to that node to calculate the current node. If this is not the case, the pre-calculation starts.

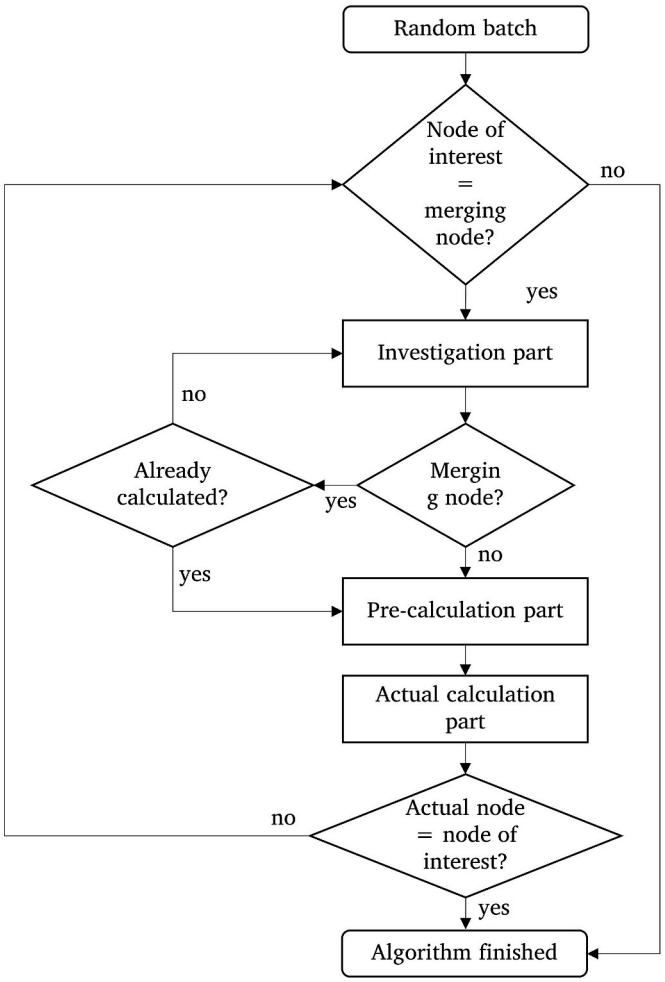

Fig. 15. Recursive algorithm.

Pre-calculation part: The task of the pre-calculation is to calculate all possible batches which can arrive at the node of interest. To do this, it uses the information generated by the investigation part and stores the temperatures and timestamps of each batch when they reach the node.

Actual calculation part: With the stored data of the pre-calculation part, the new batches can be calculated from all incoming batches using the merging rules described in Section 5.1.3. Afterwards, the newly created batches are moved further to the following nodes, following the rules described in Section 5.1.2.

6. Convergence and pressure calculation

Once the batches are created and pushed through the network, the calculated node temperatures from the temperature calculation of chapter 4.3 are compared to the temperatures of the previous iteration step. If the temperature of the current iteration step does not converge with the previous one, a new iteration step at the same time step starts. For an accurate calculation, the volume flow rate in Eqs. (4-1) is calculated with the average node temperatures from the batch calculation (Eqs. (5-4)) for all iteration steps except for the first iteration step (initial parameters are used for this step).

At the end of each time step, it is checked if there are any batches with the same rear temperature as the front temperature of the next batch. If this is the case, these batches are combined.

A pipe pressure calculation is performed at the end of each time step to ensure that the pipes operate within their pressure limits. This is used to determine the pressure at each node of the network. It takes into account the altitude meters. If the pressure exceeds or falls below the respective limitation, the calculation issues a warning, noting that the pipes must be selected differently.

7. Validation

The presented plug-flow method for district heating networks was developed to calculate entire highly branched networks using a Lagrangian specification approach. The calculation method should also be able to incorporate various elements of the district heating network. For this reason, two validation scenarios were performed. One validates the functionality of the steady-state part of the calculation considering the implementable elements of Chapter 4.2.1. In the second validation, the results of the quasi-dynamic LFC are compared to the measured data of an existing network. To measure the quality of the presented method, validation scenario 2 is analysed with the mean absolute percentage error (MAPE). This key performance indicator (KPI) can be used when comparing different forecast models or data sets. It is calculated as shown in Eqs. (7-1). Where y' is the calculated value, y the measured value, N the number of time steps and z the current time step [47].

$$MAPE = \frac{1}{N} \sum_{z=1}^{z=n} \frac{|y' - y|}{y} \bullet 100 \quad (7\text{-}1)$$

To evaluate the MAPE, Swanson [48] categorizes the results of this KPI for forecasting methods. These categories are rearranged in this paper to evaluate the accuracy of load flow calculations. The smaller the MAPE, the more accurate the method [48]. Table 3 shows the evaluation index based on the MAPE.

Table 3
Evaluation index.

Evaluation index	MAPE %
Perfect accuracy	0
High and acceptable accuracy	<5
Low but acceptable accuracy	5–25
Very low and not acceptable accuracy	>25

7.1. Validation scenario 1

During the first validation, the example network is in a steady state since the dynamic calculation provided by Roka[3] [49] has not yet been validated at the time of writing, according to the manufacturers [50]. This validation scenario aims to determine the functionality of the steady-state part (including some of the described elements from Chapter 4.2.1) of the presented method and to test its accuracy. Fig. 16 shows the network which is used in the first validation. Node 1 is the slack node, and node 15 corresponds to a heat pump in the feed flow. A pressure pump is installed at node 14, which raises the pressure by 0.5 bar in the feed flow. All other twelve nodes correspond to consumer nodes with different consumer power demands. The specific network input data is described in the Appendix.

The temperatures of the results from Roka[3] and the method presented in this paper are compared in Table 4 for the feed flow. The negligibly low differences are because Roka[3] uses temperature-dependent values for density and heat capacity in its calculations. As expected the results of node 15 show an increasing temperature due to the heat pump.

The pressure increase at node 14 corresponds to the defined 0.5 bar, in agreement with the intended function of the pressure pump element. The produced power at the slack node 1 is 2,412,054 W in Roka[3] and 2,412,218 W in the presented method. This corresponds to a relative difference of 0.0068%. This difference arises most likely from the temperature-dependent values in Roka[3]. The results of the return flow temperatures are shown in the appendix in Table A4. The differences between the temperatures of the two calculation types are also negligibly low in the return flow.

7.2. Validation scenario 2

In the second validation scenario, the presented calculation method is compared with an existing district heating network (Fig. 17). For this purpose, the measured data of the existing network were analysed and prepared to be used for the calculation in the presented method. The network consists of one producer node (node 32) and 25 consumer nodes. The branch nodes always represent either branches or a change in the pipe type. The specific input data may not be published for data protection reasons. The network data originate from 2014/2015, where the measured consumption data of node 10 were recorded only in unusable form due to technical failures. To compensate for this error in the best possible way, this node was fed with the data of another node with a similar connected load power. Measurement errors also occur at irregular intervals at different nodes. For a validation run, however, good measurement data of half a day is sufficient to obtain meaningful results since a typical temperature batch traverses the entire network in one to two hours, depending on the consumer power. For this reason, the network was simulated for the period of the night of December 02, 2014 from 18:15 to 6:15. No measurement errors are expected for this period after thorough troubleshooting. However, not all measurement errors of the installed flowmeters and heat meters can be entirely excluded based on the analysis of the available data alone. This is because errors can always occur in actual operations that could go unnoticed when simply looking at the data. The time step interval is 15 min, in line with the 15-min resolution of the measurement data. Due to this time resolution, several previous time steps affect the time step under consideration. For this reason, this use case is ideal for validating a dynamic or quasi-dynamic approach. Furthermore, a steady-state approach would not be able to calculate the example network in this time resolution in individual cases since, in some time steps, the high temperature of previous time steps in the feed flow is needed to obtain a higher feed flow temperature at a consumer than the measured/required return flow temperature. This situation occurs, e.g., at node 29 at time step 3. However, this case will not be discussed in detail here since this scenario is about validating the quasi-dynamic approach.

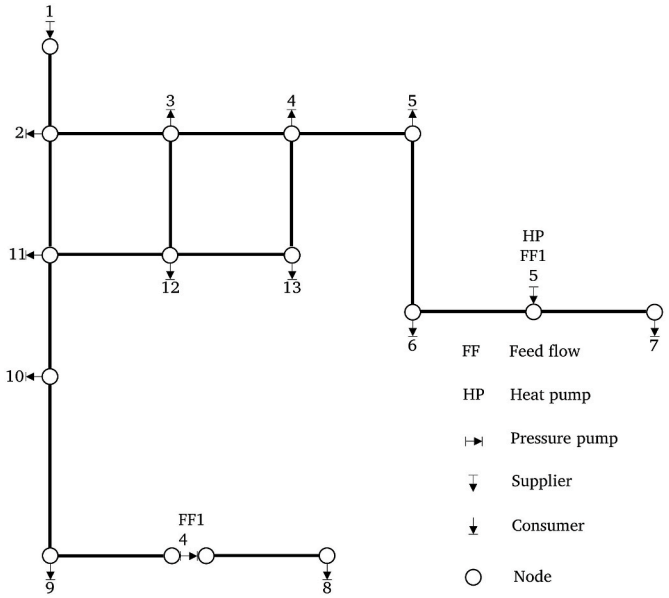

Fig. 16. Validation network 1.

Table 4
Validation 1: Feed flow Temperatures.

Node	Temperature feed flow in °C		
	Roka[3]	Method of this paper	Difference
1	85.000	85.000	0.000
2	84.791	84.790	0.001
3	84.614	84.613	0.001
4	83.829	83.828	0.001
5	83.467	83.465	0.002
6	81.793	81.802	0.009
7	85.457	85.464	0.007
8	83.083	83.080	0.004
9	83.574	83.573	0.002
10	84.157	84.155	0.002
11	84.626	84.625	0.001
12	83.801	83.804	0.003
13	83.336	83.339	0.003
14	83.328	83.826	0.002
15	85.809	86.816	0.008

For the validation, the measured consumer power is used as input data for the presented quasi-dynamic load flow calculation. Based on this input, the generation power of the producer is calculated and compared to the measured generation power, as shown in Fig. 18. The producer- and consumer power is determined from the measured data as shown in Eqs. (7-2).

$$\dot{Q} = \dot{V}_{meas} \bullet \rho \bullet c_p \bullet \left(T_{FF,meas} - T_{RF,meas}\right) \tag{7-2}$$

In most cases, the calculated generation power matches the measured power. The mean absolute percentage error between the calculated and prepared power time series is 3.7% for the calculated period. Based on the defined evaluation index, shown in Table 3, the MAPE of the presented method corresponds to a high and thus acceptable accuracy. More significant differences (as in time steps 7, 15, 17, 19, 23, 31, 44) most likely result from the exchanged data of node 10, which were replaced by similar data of another node due to technical measurement problems. Also, as already mentioned, temperature and flow meter errors cannot be excluded entirely, which can also cause differences between the measured and calculated power time series. Fig. 17 shows a clear gap between the total power required by the consumers and the power generated by the producer. This gap results from heat losses. The change in the size of this gap over time depends on

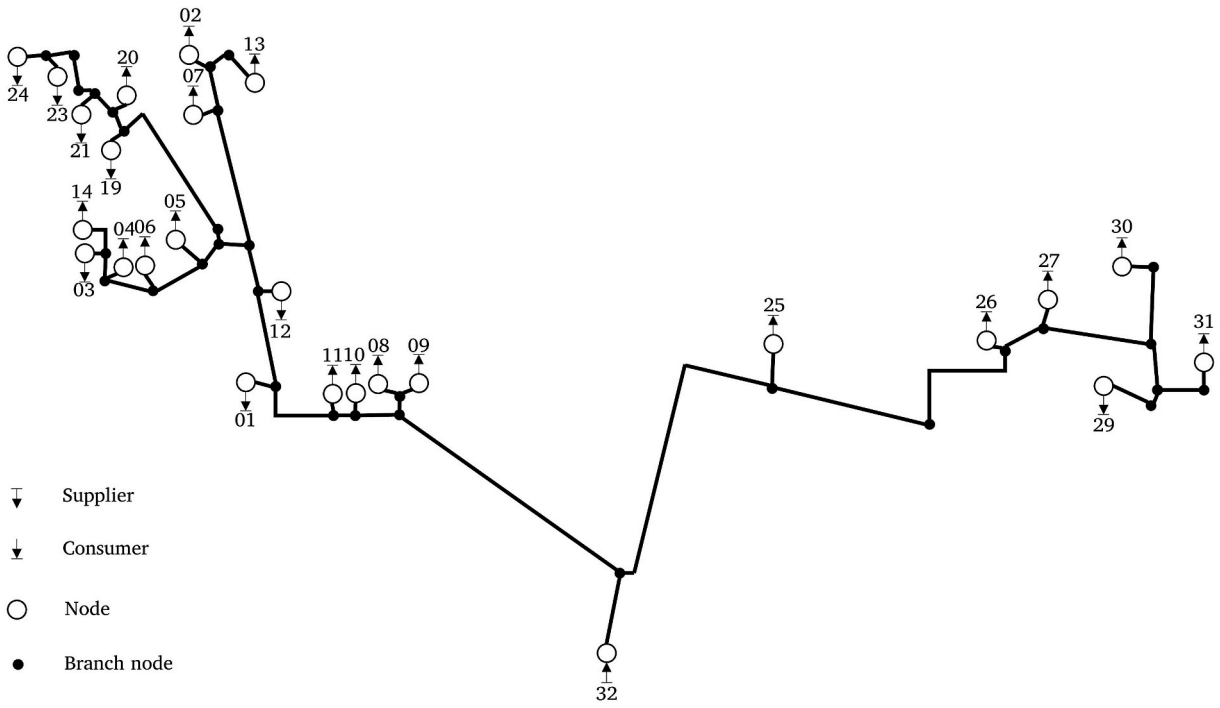

Fig. 17. Validation network 2.

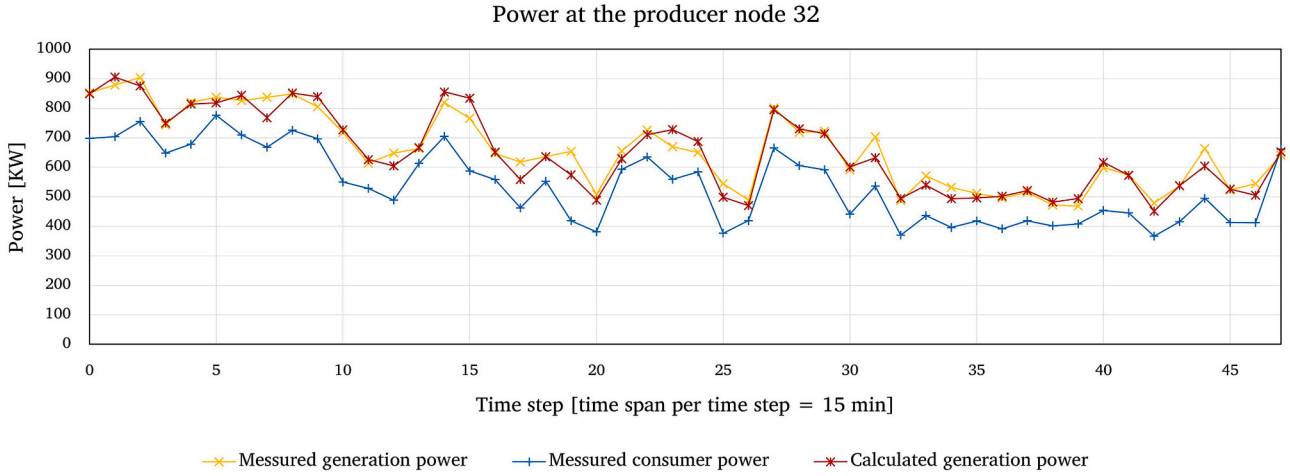

Fig. 18. Validation 2: Comparison of the producer power.

the different power consumption of the different consumer nodes at different times. Minor differences between producers and consumers can be explained by the fact that the network can act as heat storage and thus use heat surpluses from previous time steps. The fact that this behaviour can be observed in the quasi-dynamic calculation is an essential indicator that the quasi-dynamic calculation works. It also shows the advantages of dynamic calculation over steady-state calculation approaches since the latter cannot reproduce such behaviour.

In addition to the reasons mentioned above for deviations, it must be taken into account that the actual behaviour of different components can only be represented to a certain degree in the calculation to keep the computational effort within limits. The calculation of the steady-state part takes only some milliseconds per time step in this validation scenario. The whole calculation (including the quasi-dynamic part) takes up to one second per time step, depending on the producer and consumer behaviour at each time step. The computing time of each time step is shown in Table A5 in the appendix for this validation scenario.

7.3. Computational time

The program code's runtime depends mainly on how many batches (due to temperature fluctuations at the producer nodes) are in the network. The more batches are in the network, the more batches have to be moved, which is reflected in the computing time. There will be fewer batches if the input data changes less or does not change. This is because the batches of different time steps can be combined if the front temperature of one batch and the rear temperature of the batch in front of the previous batch have the same value. The specification of the accuracy and the resulting iteration steps also significantly influence the runtime. The complexity of the topology of the district heating network also has an impact on computing time. To evaluate the computational time, the presented method based on a quasi-dynamic approach is compared with a method which is close to a fully dynamic approach and the steady-state part of the presented paper. Therefore, the validation network "Pongau", shown in Ref. [29] with a network length of 298 m,

was calculated based on the information described. Due to the only schematically presented network operation information in Ref. [29], it was only possible to approximate the generation and consumption profile. In the work of B. van der Hejide et al. [29], a method based on the dynamic pipe model from the Modelica Standard Library (MSL) version 3.2.2 for the calculation of the validation network "Pongau" is presented. Here, the pipes are divided into sections of 1 m, which is close to a fully dynamic method (there, the temperature distribution in each part of the network should be known in a very high resolution, as described in chapter 1.1). The results of the comparison are shown in Table 5. To calculate the respective computing time, the validation network was simulated in 50 runs, and the central processing unit (CPU) time was measured. Each simulation run was performed with 168 time steps.

This validation was done with a Lenovo ThinkPad T14 device with six cores of an AMD Ryzen™ 5 PRO 4650U 2.10 GHz Processor. It has 16 GB RAM and runs Windows 10.

7.4. Discussion

Based on the validation and literature review results, the three described approaches (steady-state, quasi-dynamic and dynamic) are suitable for different use cases, as shown in the following paragraphs.

The steady-state approach has the lowest computing time, according to Table 5. The results of validation scenario 2 show that steady-state methods are unsuitable for LFC with low time step duration due to the described situation at node 29 at time step 3. The overall reason for this is that steady-state methods cannot consider temperature distribution in district heating networks. Concluding from this, this approach is recommended for the following use cases:

- For calculations where the heat network is completely flowed through in one time step.
- For the design of networks where a steady-state of the network can be assumed.
- As part of a calculation method for multi-energy-systems where bullet point one is fulfilled and the overall calculation time should be short. The storage effect of the DHN would be neglected in this case. For this reason, this approach is not ideal for MES calculation.

The computing time for quasi-dynamic approaches is slightly higher than for steady-state approaches but 45 times lower than for dynamic approaches. This behaviour of the computation time is described in the literature and is also demonstrated in this thesis in chapter 7.3. With a low MAPE of 3.7%, the accuracy of the presented quasi-dynamic approach is, according to the evaluation index (Table 3), high and thus acceptable accurate. Which belongs to the second-best category after perfect accuracy. Whereby a perfect accuracy with a MAPE of 0% is almost impossible to achieve. The major advantage of the quasi-dynamic approaches is that they can take into account the thermal inertia of the DHN and thus, the temperature distribution at the nodes based on the temperature variations at the generators. If the applied method is capable of solving highly branched meshes, as it is the case with the presented method (which is one of the major innovations of this paper, among others), the quasi-dynamic approach is suitable for the following use cases:

Table 5
Comparison of the performance of different approaches.

Approach	Average CPU time in seconds
Steady-state	1.09
Quasi-dynamic (This paper)	2.89
Dynamic (MSL)	130.25

- The calculation of complex or less complex, small or large DHN with arbitrary time step duration.
- As a part of the calculation method for MES.

Dynamic approaches have the highest calculation time. Due to the high resolution of the temperature distribution they are recommended for the following applications:

- For calculating the thermal properties of pipes used in DHN.
- To calculate the thermal behaviour of small DHN.

Table 6 shows the recommended applicability of the different approaches based on the validation results and literature.

8. Conclusions and future outlook

The presented paper proposes a quasi-dynamic load flow calculation approach for entire district heating networks. Based on a steady-state heat load flow calculation, which uses a modified potential node method from electric systems, the calculation is extended to a quasi-dynamic approach by integrating temperature batches. What finally corresponds to an improved plug-flow method. The developed method provides the ability to consider temperature and power changes at different time steps and assess the effects of these changes. This approach makes it possible to solve real-world load flow problems with high accuracy, and by avoiding differential equations, the computation time can be kept low.

In summary, the main findings of this work can be described as follows:

- The presented method allows the computation of any given DHN with high accuracy and good computational performance. The inertia of the DHN, which plays a crucial role in heat networks, is also taken into account.
- The results of this work show that quasi-dynamic approaches are the best approach to use in MES computation tools. The presented method is particularly suitable due to its versatility, as it can take into account all possible elements of a DHN, such as sector coupling elements.

Based on future work, a reduction in the computational time of the method is very likely. In the future, the heat load flow calculation should be extended to include operating and installation costs. For this purpose, it will be necessary to integrate an operating strategy that decides which elements should preferably be used in the respective time step based on their costs. The method should allow a more accurate techno-economic analysis of different heat networks, as it can take advantage of the quasi-dynamic LFC (taking into account the temperature distribution, which leads to a more accurate calculation). Furthermore, the load flow calculation should be integrated into a hybrid load flow calculation to consider other energy sources, such as electricity and gas, in the technical-economic analysis.

Credit author statement

Josef Steinegger: Conceptualization, Literature research, Methodology, Software, Validation, Writing - Original Draft, Visualization. **Thomas Kienberger**: Conceptualization, Writing - Review & Editing, Supervision. **Matthias Greiml**: Methodology. **Stefan Wallner**: Methodology.

Funding

This project received funding from the Austrian Climate and Energy Funds and the State of Upper Austria (project "Heat Highway", FFG-number 880797).

Table 6
Recommended application of the different approaches.

Approach	Type of application						
	Pipe designing	Network designing	Single pipes	Small DHN	Big DHN	Complex DHN	MES
Steady-state	-	+	-	~	~	~	~
Quasi-dynamic	-	-	-	+	+	+	+
Dynamic	+	-	+	~	-	-	-

+ Recommendable/~ Possible under certain conditions/- Not recommendable.

Declaration of competing interest

The authors declare that they have no known competing financial interests or personal relationships that could have appeared to influence the work reported in this paper.

Data availability

The data that has been used is confidential.

Appendix. 11

Table A1 shows the input data of all nodes from the sample network described in Chapter 7.1.

Table A1
Node input data

Node ID	Power	Temperature	Pressure
	W	°C	Pa
1	–	85 (feed flow)	800,000
2	45,000	55 (return flow)	–
3	30,000	55 (return flow)	–
4	200,000	55 (return flow)	–
5	50,000	55 (return flow)	–
6	40,000	55 (return flow)	–
7	700,000	55 (return flow)	–
8	900,000	55 (return flow)	–
9	20,000	55 (return flow)	–
10	40,000	55 (return flow)	–
11	50,000	55 (return flow)	–
12	60,000	55 (return flow)	–
13	90,000	55 (return flow)	–
14	–	55 (return flow)	Δ50000
15	100,000	100 (feed flow)	–

Table A2 shows the input data of all pipes in the sample network described in Chapter 7.1.

Table A2
Pipe input data

Pipe ID	From node	To node	Pipe diameter m	Pipe length m	Wall roughness m	Heat transmittance coefficient • scope W/mK
1	1	2	0.2111	500	0.0001	0.09882
2	2	3	0.2111	200	0.0001	0.09882
3	2	11	0.2111	200	0.0001	0.09882
4	3	4	0.2111	200	0.0001	0.09882
5	3	12	0.2111	200	0.0001	0.09882
6	4	13	0.2111	200	0.0001	0.09882
7	4	5	0.2111	300	0.0001	0.09882
8	5	6	0.2111	1300	0.0001	0.09882
9	6	15	0.2111	251	0.0001	0.09882
10	13	12	0.2111	200	0.0001	0.09882
11	12	11	0.2111	200	0.0001	0.09882
12	11	10	0.2111	500	0.0001	0.09882
13	10	9	0.2111	600	0.0001	0.09882
14	9	14	0.2111	251	0.0001	0.09882
15	14	8	0.2111	249	0.0001	0.09882
16	15	7	0.2111	249	0.0001	0.09882

Table A3 shows the remaining selected properties in the sample network.

Table A3
Remaining properties

Property	Value	Unit
kinematic viscosity	$1.1 \bullet 10^{-6}$	m^2/s
density	978	kg/m^3
heat capacity	4190	J/kgK
ambient temperature	6.6	°C

Table A4 shows the return flow temperatures from the validation scenario 1

Table A4
Validation 1: Return flow temperatures

Node	Temperature return flow in °C		
	Roka[3]	Method of this paper	Difference
1	53.573	53.574	0.001
2	53.698	53.700	0.002
3	53.551	53.554	0.003
4	53.755	53.760	0.005
5	53.647	53.653	0.006
6	54.595	54.595	0.000
7	55.000	55.000	0.000
8	55.000	55.000	0.000
9	54.697	54.697	0.000
10	54.362	54.362	0.000
11	53.984	53.985	0.001
12	53.680	53.682	0.003
13	53.762	53.765	0.003

Table A5 shows the computing time of the second validation scenario for each time step.

Table A5
Computing time of the validation scenario 2

Time step	CPU time in seconds	Real calculating time in seconds
1	0.671875	0.4646616
2	0.765625	0.6107829
3	0.890625	0.4680094
4	1.125000	0.8845147
5	1.187500	0.6531411
6	0.625000	0.6160931
7	1.234375	0.8734283
8	0.687500	0.5786707
9	0.656250	0.4926179
10	1.031250	0.6605790
11	0.718750	0.6485085
12	0.921875	0.6408590
13	0.671875	0.4774609
14	1.093750	0.6349016
15	0.593750	0.4737051
16	1.343750	0.6495286
17	1.281250	0.5971067
18	0.765625	0.5105059
19	0.984375	0.4291154
20	1.078125	0.6448237
21	0.921875	0.4564717
22	0.890625	0.4908575
23	0.468750	0.4827642
24	0.593750	0.4772966
25	1.000000	0.6476767
26	0.468750	0.4404601
27	0.687500	0.6385784
28	0.906250	0.4860927
29	1.203125	0.4498117
30	0.671875	0.5461620
31	0.890625	0.4771090
32	0.921875	0.4636888
33	0.765625	0.4841977
34	0.890625	0.6344883
35	0.828125	0.5374730
36	1.093750	0.5746446
37	0.734375	0.4814903
38	0.796875	0.6795039

(*continued on next page*)

Table A5 (*continued*)

Time step	CPU time in seconds	Real calculating time in seconds
39	0.593750	0.4179403
40	0.937500	0.5743902
41	0.984375	0.6452292
42	1.062500	0.4381585
43	0.500000	0.3988432
44	0.843750	0.7711376
45	0.703125	0.5807801
46	0.484375	0.4462539
47	0.515625	0.4333113
48	0.640625	0.4328867

References

[1] Intergovernmental Panel on Climate Change. Climate Change. Impacts, adaptation and vulnerability. IPCC WGII sixth assessment report. https://www.ipcc.ch/report/ar6/wg2/downloads/report/IPCC_AR6_WGII_FinalDraft_FullReport.pdf%20-%20Review%20date. 15.07.022.

[2] European Commission. The European green deal. https://eur-lex.europa.eu/resource.html?uri=cellar:b828d165-1c22-11ea-8c1f-01aa75ed71a1.0002.02/DOC_1&format=PDF%20-%20Review%20date:%202019-07-15.

[3] Biomasse-Verband Österreichischer. Bioenergie: basisdaten 2021. https://www.biomasseverband.at/wp-content/uploads/Basisdaten-Bioenergie-2021.pdf%20-%20Review%20date:%202022-08-02.

[4] Bundeskanzleramt. Aus Verantwortung für Österreich: regierungsprogramm 2020-2024. https://www.bundeskanzleramt.gv.at/dam/jcr:7b9e6755-2115-440c-b2ec-cbf64a931aa8/RegProgramm-lang.pdf%20-%20Review%20date:%202022-07-15.

[5] Abdur Rehman Mazhar, Liu Shuli, Shukla Ashish. A state of art review on the district heating systems. Renew Sustain Energy Rev 2018;96:420–39. https://doi.org/10.1016/j.rser.2018.08.005.

[6] Olsthoorn Dave, Haghighat Fariborz, Parham A. Mirzaei. Integration of storage and renewable energy into district heating systems: a review of modelling and optimization. Sol Energy 2016;136:49–64. https://doi.org/10.1016/j.solener.2016.06.054.

[7] Lund H, Möller B, Mathiesen BV, Dyrelund A. The role of district heating in future renewable energy systems. Energy 2010;35:1381–90. https://doi.org/10.1016/j.energy.2009.11.023.

[8] Guelpa Elisa. Impact of network modelling in the analysis of district heating systems. Energy 2020;213:118393. https://doi.org/10.1016/j.energy.2020.118393.

[9] Dancker Jonte, Wolter Martin. Improved quasi-steady-state power flow calculation for district heating systems: a coupled Newton-Raphson approach. Appl Energy 2021;295:116930. https://doi.org/10.1016/j.apenergy.2021.116930.

[10] Lund Henrik, Duic Neven, Poul Alberg Østergaard, Brian Vad Mathiesen. Future district heating systems and technologies: on the role of smart energy systems and 4th generation district heating. Energy 2018;165:614–9. https://doi.org/10.1016/j.energy.2018.09.115.

[11] Zhang Suhan, Gu Wei, Lu Shuai, Yao Shuai, Zhou Suyang, Chen Xiaogang. Dynamic security control in heat and electricity integrated energy system with an equivalent heating network model. IEEE Trans Smart Grid 2021;12:4788–98. https://doi.org/10.1109/TSG.2021.3102057.

[12] Dancker Jonte, Wolter Martin. A joined quasi-steady-state power flow calculation for integrated energy systems. IEEE Access 2022;10:33586–601. https://doi.org/10.1109/ACCESS.2022.3161961.

[13] Chen Dongwen, Li Yong, Zulkarnain Abbas, Li Dehong, Wang Ruzhu. Network flow calculation based on the directional nodal potential method for meshed heating networks. Energy 2022;243:122729. https://doi.org/10.1016/j.energy.2021.122729.

[14] Amin Shabanpour-Haghighi, Reza Seifi Ali. An integrated steady-state operation assessment of electrical, natural gas, and district heating networks. IEEE Trans Power Syst 2016;31:3636–47. https://doi.org/10.1109/TPWRS.2015.2486819.

[15] Liu Xuezhi, Mancarella Pierluigi. Modelling, assessment and Sankey diagrams of integrated electricity-heat-gas networks in multi-vector district energy systems. Appl Energy 2016;167:336–52. https://doi.org/10.1016/j.apenergy.2015.08.089.

[16] Shi Jiaqi, Wang Ling, Wang Yingrui, Zhang Jianhua. Generalized energy flow analysis considering electricity gas and heat subsystems in local-area energy systems integration. Energies 2017;10:514. https://doi.org/10.3390/en10040514.

[17] Liu Xuezhi, Wu Jianzhong, Jenkins Nick, Audrius Bagdanavicius. Combined analysis of electricity and heat networks. Appl Energy 2016;162:1238–50. https://doi.org/10.1016/j.apenergy.2015.01.102.

[18] Reza Massrur Hamid, , Niknam Taher, Jamshid Aghaei, Miadreza Shafie-khah, Catalao Joao PS. Fast decomposed energy flow in large-scale integrated electricity–gas–heat energy systems. IEEE Trans Sustain Energy 2018;9:1565–77. https://doi.org/10.1109/TSTE.2018.2795755.

[19] Zhang Suhan, Gu Wei, Yao Shuai, Lu Shuai, Zhou Suyang, Wu Zhi. Partitional decoupling method for fast calculation of energy flow in a large-scale heat and electricity integrated energy system. IEEE Trans Sustain Energy 2021;12:501–13. https://doi.org/10.1109/TSTE.2020.3008189.

[20] Jia Mengshuo, Huang Shaowei, Tang Kexuan, Chen Shen. An investigation on the applicability of the integrated method for multi-carrier energy flow analysis. IEEE Power & Energy Society General Meeting (PESGM); 2018. https://doi.org/10.1109/PESGM.2018.8585831. 1–5.

[21] Heleno Miguel, Ren Zhengwei. Multi-energy microgrid planning considering heat flow dynamics. IEEE Trans Energy Convers 2021;36:1962–71. https://doi.org/10.1109/TEC.2020.3041572.

[22] Yang Wentao, Wen Fushuan, Wang Ke, Huang Yuchun, Md. Salam. Modeling of a district heating system and optimal heat-power flow. Energies 2018;11:929. https://doi.org/10.3390/en11040929.

[23] Markensteijn AS, Romate JE, Vuik C. A graph-based model framework for steady-state load flow problems of general multi-carrier energy systems. Appl Energy 2020;280:115286. https://doi.org/10.1016/j.apenergy.2020.115286.

[24] Pan Zhaoguang, Guo Qinglai, Sun Hongbin. Interactions of district electricity and heating systems considering time-scale characteristics based on quasi-steady multi-energy flow. Appl Energy 2016;167:230–43. https://doi.org/10.1016/j.apenergy.2015.10.095.

[25] Pan Zhaoguang, Wu Jianzhong, Sun Hongbin, Guo Qinglai, Muditha Abeysekera. Quasi-dynamic interactions and security control of integrated electricity and heating systems in normal operations. CSEE J Power Energy Syst 2019;295:116930. https://doi.org/10.17775/CSEEJPES.2018.00240.

[26] Oppelt T, Urbaneck T, Gross U, Platzer B. Dynamic thermo-hydraulic model of district cooling networks. Appl Therm Eng 2016;102:336–45. https://doi.org/10.1016/j.applthermaleng.2016.03.168.

[27] Thomas Oppelt. Modell zur Auslegung und Betriebsoptimierung von Nah- und Fernkältenetzen. Dissertation. Chemnitz. Selbstverlag der Professur Technische Universität Chemnitz; 2015. 978-3-9811424-6-4.

[28] Dénarié A, Aprile M, Motta M. Heat transmission over long pipes: new model for fast and accurate district heating simulations. Energy 2019;166:267–76. https://doi.org/10.1016/j.energy.2018.09.186.

[29] van der Heijde B, Fuchs M, Ribas Tugores C, Schweiger G, Sartor K, Basciotti D, Müller D, Nytsch-Geusen C, Wetter M, Helsen L. Dynamic equation-based thermo-hydraulic pipe model for district heating and cooling systems. Energy Convers Manag 2017;151:158–69. https://doi.org/10.1016/j.enconman.2017.08.07.

[30] Benedikt Leitner, Widl Edmund, Gawlik Wolfgang, Hofmann René. A method for technical assessment of power-to-heat use cases to couple local district heating and electrical distribution grids. Energy 2019;182:729–38. https://doi.org/10.1016/j.energy.2019.06.016.

[31] Benonysson Atli. Dynamic modelling and operational optimization of district heating systems. Lyngby, Techn. Univ. of Denmark, Ph. D. Thesis; 1991. https://www.osti.gov/etdeweb/biblio/10133561%20-%20Review%20date:%202022-07-21.

[32] Qin Xin, Sun Hongbin, Shen Xinwei, Guo Ye, Guo Qinglai, Tian Xia. A generalized quasi-dynamic model for electric-heat coupling integrated energy system with distributed energy resources. Appl Energy 2019;251:113270. https://doi.org/10.1016/j.apenergy.2019.05.073.

[33] Qin Xin, Shen Xinwei, Sun Hongbin, Guo Qinglai. A quasi-dynamic model and corresponding calculation method for integrated energy system with electricity and heat. Energy Proc 2019;158:6413–8. https://doi.org/10.1016/j.egypro.2019.01.195.

[34] Ben Hassine Ilyes, Ursula Eicker. Impact of load structure variation and solar thermal energy integration on an existing district heating network. Appl Therm Eng 2013;50:1437–46. https://doi.org/10.1016/j.applthermaleng.2011.12.037.

[35] Guelpa Elisa, Vittorio Verda. Compact physical model for simulation of thermal networks. Energy 2019;175:998–1008. https://doi.org/10.1016/j.energy.2019.03.064.

[36] Stevanovic VD, Zivkovic B, Prica S, Maslovaric B, Karamarkovic V, Trkulja V. Prediction of thermal transients in district heating systems. Energy Convers Manag 2009;50:2167–73. https://doi.org/10.1016/j.enconman.2009.04.034.

[37] Wang Yaran, You Shijun, Zhang Huan, Zheng Xuejing, Zheng Wandong, Miao Qingwei, Lu Gang. Thermal transient prediction of district heating pipeline: optimal selection of the time and spatial steps for fast and accurate calculation. Appl Energy 2017;206:900–10. https://doi.org/10.1016/j.apenergy.2017.08.061.

[38] Zheng Jinfu, Zhou Zhigang, Zhao Jianing, Wang Jinda. Function method for dynamic temperature simulation of district heating network. Appl Therm Eng 2017;123:682–8. https://doi.org/10.1016/j.applthermaleng.2017.05.083.

[39] Bernd Glück. Heizwassernetze für Wohn- und Industriegebiete. Frankfurt (Main): Verlag für Bauwesen; 1985. p. 3–8022.
[40] Martin Icking. Zur Modellierung des dynamischen Betriebs von Fernwärmesystemen. Zugl.: dortmund, Univ., Diss.. first ed. Konstanz: Hartung-Gorre; 1994, 3891919522.
[41] Jens Rüdiger. Enhancements of the numerical simulation algorithm for natural gas networks based on node potential analysis. IFAC-PapersOnLine 2020;53:13119–24. https://doi.org/10.1016/j.ifacol.2020.12.2282.
[42] Greiml Matthias, Fritz Florian, Steinegger Josef, Schlömicher Theresa, Williams Wolf Nicholas, Zaghi Negar, Kienberger Thomas. Modelling and simulation/optimization of Austria's national multi-energy system with a high degree of spatial and temporal resolution. Energies 2022;15:3581. https://doi.org/10.3390/en15103581.
[43] Lund Henrik, , Poul Alberg Østergaard, Chang Miguel, Werner Sven, Svendsen Svend, Peter Sorknæs, , Jan Eric Thorsen, Hvelplund Frede, , Bent Ole Gram Mortensen, Vad Mathiesen Brian, Bojesen Carsten, Duic Neven, Zhang Xiliang, Möller Bernd. The status of 4th generation district heating: research and results. Energy 2018;164:147–59. https://doi.org/10.1016/j.energy.2018.08.206.
[44] Bucar G, Schweyer K, Fink C, Riva R, Neuhäuser M, Meissner E, Streicher W, Halmdienst C. Dezentrale erneuerbare Energie für bestehende Fernwärmenetze: berichte aus Energie- und Umweltforschung. Innovation und Technologie: Bundesministeriums für Verkehr; 2005. Wien.
[45] Klaus Langeheincke, Peter Jany, Gerd Thieleke, Kay Langeheincke, Kaufmann Andre. Thermodynamik für Ingenieure. Wiesbaden: Springer Fachmedien Wiesbaden; 2013. 978-3-658-03168-8.
[46] Munavalli GR, Mohan Kumar MS. Modified Lagrangian method for modeling water quality in distribution systems. Water Res 2004;38:2973–88. https://doi.org/10.1016/j.watres.2004.04.007.
[47] Swanson David A, Tayman Jeff, Bryan TM, Mape-R. A rescaled measure of accuracy for cross-sectional subnational population forecasts. J Popul Res 2011;28:225–43. https://doi.org/10.1007/s12546-011-9054-5.
[48] Swanson David A. On the relationship among values of the same summary measure of error when used across multiple characteristics at the same point in time: an examination of MALPE and MAPE. Review of economics and finance. 2015. https://escholarship.org/uc/item/1f71t3x9.
[49] RZVN Wehr GmbH. Roka^3. https://www.roka3.de/-%20Review%20date:%202022-08-25.
[50] Employee of Rechenzentrum für Versorgungsnetze Wehr GmbH. Roka^3 - dynamic calculation. by phone: 2022-08-10. Josef steinegger (interlocutor).